Filling the Gap: Hunting for Vector Bosons at the MUonE Experiment with Displaced Decay Signature

Duncan Rocha^a Isaac R. Wang^b

^aEnrico Fermi Institute, University of Chicago, Chicago, IL USA

E-mail: drocha@uchicago.edu, isaacw@fnal.gov

ABSTRACT: The upcoming MUonE experiment aims to precisely measure the running of the fine structure constant via elastic muon-electron scattering, to shed light on the current tension in the muon's anomalous magnetic moment. In addition to its primary function as a precision experiment, MUonE also offers a unique testing ground to probe long-lived vector bosons. Such vector bosons can be produced via $\mu e \to \mu eV$ or $\mu N \to \mu NV$ scattering and decay into an electron/positron pair a few centimeters away from the interaction point. With its high-resolution tracking system and unique geometric design, MUonE is well-suited to reconstruct displaced vertices close to the target, allowing it to probe parameter space previously unattainable at colliders and longer-baseline beam dump experiments. We present a comprehensive study of the discovery potential of BSM vector boson mediators at the MUonE experiment. We show that MUonE can fill the long-standing gap in the parameter space of vector boson mediators with masses up to around 100 MeV.

^b Theoretical Physics Division, Fermi National Accelerator Laboratory, Batavia, IL, USA

\mathbf{C}	ontents	
1	1	
2	Simple Models of Vector Boson Mediators	2
3	Vector Boson Signatures at the MUonE Experiment	4
	3.1 The Apparatus	4
	3.2 Search Strategy	6
	3.3 Signal Event Generation	7
	3.4 Backgrounds	10
4	Analysis and Results	11
	4.1 Dark photon model	12
	4.2 The gauged $U(1)_{B-L}$ model	13
	4.3 The gauged $U(1)_{L_e-L_\mu}$ model	14
5	Conclusion	15

1 Introduction

Since the development of the Standard Model (SM), numerous Beyond-Standard-Model (BSM) force carriers have been proposed, including the dark photon [1–5], gauged lepton number [6–8], gauged B-L [9, 10], extra scalars [11–18], along with other scenarios. Beyond serving as simple extensions to the SM, hidden forces can address several open questions in modern physics. In particular, a hidden force mediator coupled to a dark sector can naturally account for the observed abundance of dark matter through the thermal freeze-out mechanism [19–26]. It remains undetermined whether any hidden forces exist in nature, although many experiments have been conducted to probe such models. If produced in an experiment, hidden forces could manifest in one of three possible regimes. In one regime, the mediators decay back to SM particles promptly, requiring a resonance search. If there are dark sector particles less massive than the mediator, the mediator may instead decay into the dark sector invisibly, requiring a search for missing energy. Most relevant for this work is the regime where the mediator decays visibly at a location displaced from the interaction point, requiring precise vertex reconstruction to detect. See Ref. [27–30] for systematic studies.

Interestingly, an experimental "gap" exists in parameter space where the hidden force coupling is too small for the mediator to be produced at colliders, but it also is not long-lived enough to provide a signal in existing beam dump experiments. For characteristic beam energies of $\mathcal{O}(100)\,\mathrm{GeV}$, a hidden boson in the "gap" would produce a displaced

vertex a few centimeters away from the interaction point, and thus requires a compact detector geometry to be identified.

The MUonE experiment [31, 32] was recently shown to be sensitive to the dark photon model in the "gap" [33]. MUonE was originally proposed to measure elastic μe scattering and extract the hadronic vacuum polarization contribution to the running of α . To make this measurement, MUonE has developed a tracking system capable of reconstructing charged tracks with precise angular resolution [31, 32]. This state-of-the-art tracking system also enables MUonE to detect displaced vertices, making it a promising platform for a long-lived particle search. Ref. [33] studied dark photon production through $\mu e \to \mu e A'$ with $A' \to e^+e^-$, considering both a 4-track search including all final state leptons and a 3-track search where the primary electron need not be observed. Using a simulation-based analysis, they illustrated that MUonE can probe regions in the "gap" for dark photon masses up to 70 MeV.

Importantly, Ref. [33] showed that the SM background can still be identified and rejected even if the primary electron is not detected, which opens a new possibility of considering the elastic production channel where a muon scatters off the nucleus and radiates a dark vector boson. The much larger center-of-mass (CoM) energy in μN scattering over μe can significantly enhance the maximum vector boson mass observable at MUonE. This was previously applied to show that MUonE is sensitive to inelastic dark matter in the "gap" up to 700 MeV [34].

At the time of writing this paper, MUonE finished its test run and is currently analyzing the data collected. The next stage is an official run of the experiment, projected to begin in early 2027 [35]. This recent progress calls for a detailed assessment of the sensitivity of MUonE to hidden force models. In this work, we consider three well-motivated vector boson models and generalize the displaced vertex search at MUonE to include both μN and μe scattering production channels. We conduct a simulation-based analysis and implement a search strategy following Ref. [33, 34], aimed at making reliable projections. Our main result is a characterization of the sensitivity of MUonE to the existence of a dark photon, $U(1)_{B-L}$ gauge boson, and $U(1)_{Le-L_{\mu}}$ gauge boson.

This paper is organized as follows. In Sec. 2, we provide a short review of the three models of vector boson mediators studied. In Sec. 3, we discuss how these mediators can be produced and detected at MUonE, with description of event generation and background simulation. In Sec. 4, we present the projected sensitivity curve for the three models. We conclude this paper in Sec. 5.

2 Simple Models of Vector Boson Mediators

We consider hidden force models that include a new massive U(1) vector boson V_{μ} which couples to some (or all) of the SM fermions. The interaction term in the low energy limit is

$$\mathcal{L} \supset g_V \sum_{f \in SM} c_f \bar{f} \gamma^{\mu} V_{\mu} f , \qquad (2.1)$$

where the sum is over all SM fermions. Here, $g_V c_f$ is the coupling between the massive vector boson and SM fermion f. Additional dark fermions or scalars may be present and

	g_V	c_u	c_d	$c_{ u}$	c_{ℓ}
Dark photon	ϵe	2/3	-1/3	0	-1
Gauged $L_e - L_{\mu}$	$g_{e\mu}$	0	0	$c_{\nu_e} = 1, c_{\nu_\mu} = -1, c_{\nu_\tau} = 0$	$c_e = 1, c_\mu = -1, c_\tau = 0$
Gauged $B-L$	g_{B-L}	1/3	1/3	-1	-1

Table 1: The vector boson mediator considered in this work. Columns show the notation of the coupling g_V and the charge of each SM fermions, respectively.

charged under the new hidden force, thus forming a "dark sector." We assume that any such fields are more massive than the mediator, so that the force carrier V decays only into SM products.

Notably, the list of viable U(1) gauge symmetries that can be consistently added to the SM is severely restricted by anomaly cancellation. The models we consider can all be consistently added without requiring additional fields to cancel gauge anomalies, making them well-motivated and flexible extensions of the SM.

- Dark photon: this scenario posits a $U(1)_D$ under which no SM fields are charged. However, heavy particles charged under both $U(1)_D$ and $U(1)_{EM}$ can induce a small gauge-invariant kinetic mixing term in the IR. Therefore, the mediator A'_{μ} of the $U(1)_D$ inherits the same structure of charge assignments as the SM photon [36]. It couples to all charged particles in SM with strength ϵeQ , where ϵ is the mixing parameter, e is the QED coupling, and Q is the electric charge of the charged particle.
- Gauged $U(1)_{B-L}$: this scenario gauges the existing global $U(1)_{B-L}$ symmetry in the SM [9, 10]. This avoids a gauge anomaly if one assumes right-handed neutrinos exist, and we take them to have heavy Majorana masses. The $Z'_{\mu,B-L}$ gauge boson couples to all quarks (leptons) with coupling $g_{B-L}/3$ (g_{B-L}).
- Gauged $U(1)_{L_e-L_{\mu}}$: this scenario gauges a difference of L_e and L_{μ} [6]. The $Z'_{e\mu}$ gauge boson couples to the muon (muon neutrino) and electron (electron neutrino) with coupling $\pm g_{e\mu}$, respectively. In principle, any of the three combinations can be chosen, but $U(1)_{L_e-L_{\mu}}$ is the model for which MUonE is especially sensitive.

Their properties are summarized in Table. 1.

Fig. 1 shows the Feynman diagrams for vector boson production at MUonE. All mediators can be produced by "dark bremsstrahlung" in μe or μN scattering. For μN scattering, bremsstrahlung off of the nucleus itself is severely suppressed, and thus for a given vector boson mass the cross section can be straightforwardly rescaled between models, i.e.

$$\frac{\sigma(\mu N \to \mu N V)}{\sigma(\mu N \to \mu N A')} = \frac{(g_V c_\mu)^2}{(\epsilon e)^2},$$
(2.2)

where V stands for a general vector mediator. ϵe can be any reference value in principle, and is chosen to be $\epsilon = 10^{-3}$ during the production simulation. On the contrary, vector bosons from μe scattering can be emitted from both the muon and electron legs. The

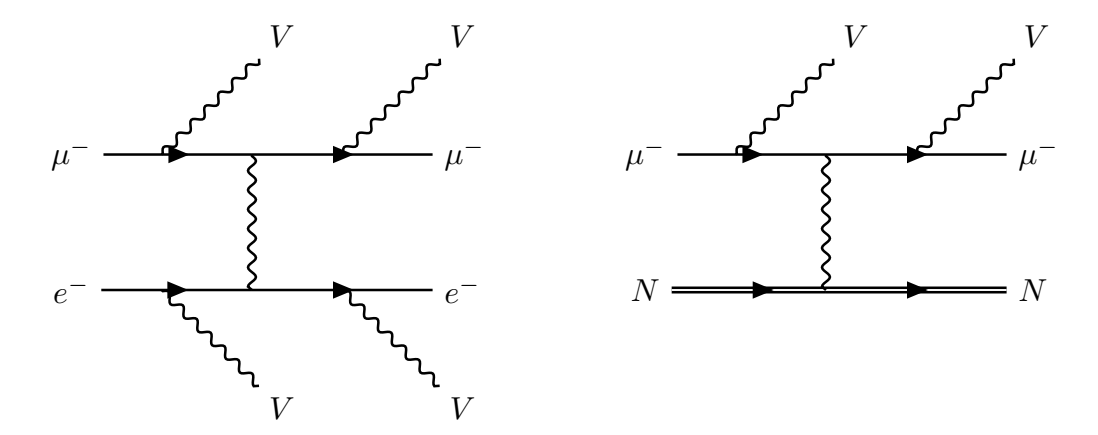


Figure 1: Feynman diagrams of vector boson production at MUonE.

interference behavior changes depending on the relative sign of the Vee and $V\mu\mu$ vertices, an effect which we find numerically to be an $\mathcal{O}(10)\%$ change in cross section. This effect can be seen in Fig. 4.

The decay rate of the vector boson V_{μ} into a pair of SM fermions in the CoM frame is

$$\Gamma_{\bar{f}f} = \frac{N_f (g_V c_f)^2}{12\pi} m_V \left(1 + \frac{2m_f^2}{m_V^2} \right) \sqrt{1 - \frac{4m_f^2}{m_V^2}}.$$
 (2.3)

In the region excluded by MUonE, the mass of the vector boson is below $2m_{\mu}$ and $2m_{\pi}$, so the only relevant decays are to electrons, neutrinos, or photons. For e and μ , $N_f = 1$. For ν , $N_f = 1/2$. Assuming only one decay channel into a pair of Dirac fermions $(N_f = 1)$ with $m_f \ll m_V$, the decay length in the lab frame is given by

$$d_V = \frac{|\vec{p}_V|}{m_V \Gamma_V} \simeq 74 \text{ mm} \left(\frac{10^{-5}}{g_V c_f}\right)^2 \left(\frac{p_V}{10 \text{ GeV}}\right) \left(\frac{100 \text{ MeV}}{m_V}\right)^2,$$
 (2.4)

where \vec{p}_V is the momentum of the vector boson in the lab frame, so that $|\vec{p}_V|/m_V$ represents the boost factor times velocity. The decay length of other vector bosons can be computed in a similar way, with the width summed over all possible final states.

3 Vector Boson Signatures at the MUonE Experiment

In this section, we introduce the signal of displaced decays of BSM vector bosons at the MUonE experiment, following Ref. [33, 34].

3.1 The Apparatus

The MUonE experiment aims to measure the hadronic vacuum polarization (HVP) contribution to the running of α [31, 32]. To do so, MUonE will follow the strategy put forth by the NA7 experiment [37, 38]. This approach uses precise measurements of the μe elastic scattering cross section to extract the HVP contribution to α , providing an important cross-check with the result from lattice QCD [39]. This quantity is crucial for making a precise

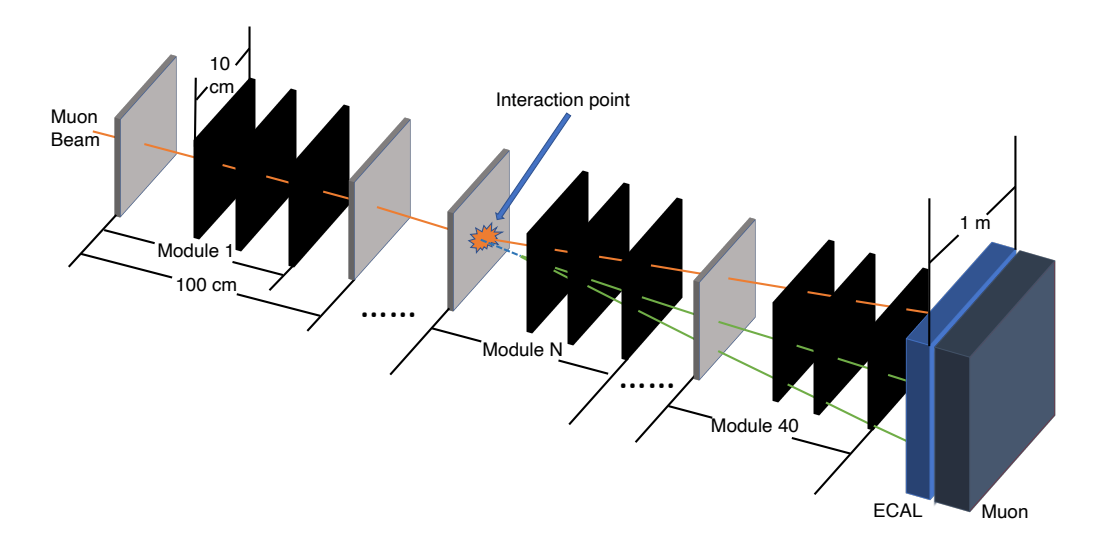


Figure 2: A schematic diagram for the MUonE apparatus with displaced vertex signature, borrowed from Fig. [34]. Orange line: incoming muon beam and outgoing scattered muon. Blue dashed line: displaced decaying vector boson. Green lines: decay products of the vector boson. Black squares: tracking stations. Gray squares: Beryllium targets. Blue and dark blue squares: the ECAL and the muon filter.

theoretical prediction of the muon anomalous magnetic moment [40, 41] and investigating the current tension with experimental measurements [42–44].

To achieve this measurement, MUonE delivers a 160 GeV muon beam from the CERN M2 beamline onto 1.5 cm thick Beryllium (Be) targets. The targets are put into 40 identical modules aligned with the beamline, each separated by 1 m. Each module contains one Be target and three $10 \text{ cm} \times 10 \text{ cm}$ tracking stations, with the first station located 15 cm away from the target. The location of the 2nd and 3rd tracking stations has not been precisely determined yet. We assume the 3rd one to be located 1 m away from the target, while the 2nd one stands in the middle between the 1st one and the 3rd one. More tracking stations may be inserted in the middle to ensure achievement of the proposed angular and vertex reconstruction resolution. At the very end of the tracking stations, an electromagnetic calorimeter (ECAL) and a muon filter with size $1 \text{ m} \times 1 \text{ m}$ are placed for the purpose of particle identification (PID). With 2 years of data taking, the proposed total luminosity is $1.5 \times 10^4 \text{ pb}^{-1}$ for μe scattering, corresponding to a total of $\sim 10^{16}$ muons on target.

The elastic $\mu e \to \mu e$ scattering can be distinguished from other events since the outgoing muon angle θ_{μ} and electron angle θ_{e} strictly follow a one-on-one correspondence, known as the elastic curve [45]. To utilize the elastic curve for background rejection, MUonE employs a CMS-based high-precision tracking system for charged track reconstruction [32, 46, 47], which achieves an angular resolution within 0.02 mrad of the outgoing particles. No magnetic field is applied, so charge discrimination and momentum measurement are not possible. The energy of the outgoing muon is not measured, and the energy resolution of the ECAL has not been finally determined yet. For this reason, a missing energy search is not possible in MUonE.

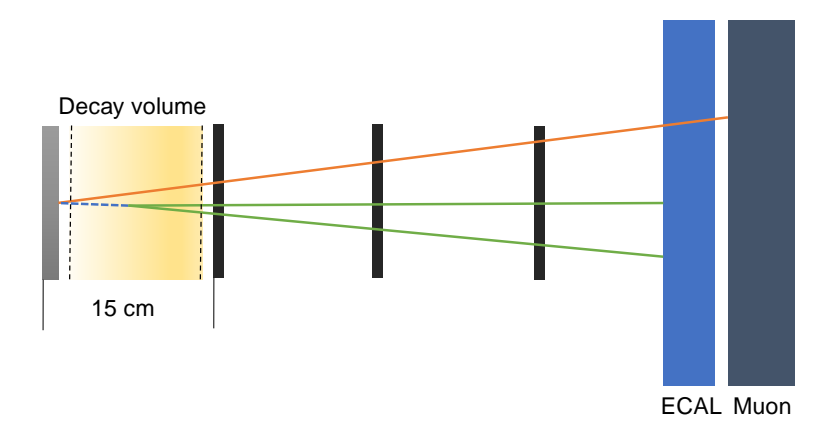


Figure 3: Signal event geometry in the corresponding volume, borrowed from Fig. [34]. We show the ECAL and muon filter after the module, but note that this can be a few meters away from the module that we consider.

Fig. 2 shows a schematic picture of the MUonE apparatus together with our proposed displaced vertex signature. The signal event topology is discussed in the next subsection.

3.2 Search Strategy

If a vector bosons from a hidden force are produced in MUonE, signal events would include a pair of charged tracks originating from a displaced vertex, corresponding to the decay of the vector boson. The final state thus contains three or four charged tracks: one coming from the primary interaction vertex, identified as the deflected muon, two reconstructed to be coming from a common displaced vertex and identified as a pair of electrons, and the potentially fourth one coming from the atomic electron that may also be involved in the production mechanism.

Fig. 3 shows the signal event process in a given module. For a successful charged track reconstruction, the tracks must pass through all three tracking stations in the module where they are produced. This requires the displaced decay to happen before the first tracking station. As shown in Ref. [33], the fourth charged track from the primary electron does not need to be observed to distinguish signal events from backgrounds, so we inclusively search for the final state with or without this electron being captured. For this reason, we do not show its track in Fig. 3. To avoid backgrounds from mis-reconstructing a prompt vertex as a displaced vertex, the displaced vertex should be at least $10\delta z$ away from both the target and the first tracking station, with $\delta z \simeq 1$ mm being the reconstruction resolution along the z direction (i.e. the streamline direction) [32–35]. The decay volume is therefore defined as

$$25 \text{ mm} \le z_{V \text{ decay}} \le 140 \text{ mm},$$
 (3.1)

where $z_{V \text{ decay}}$ stands for the decay location of the vector boson along z coordinate. We further require the decay products to have an opening angle larger than 1 mrad to ensure accurate reconstruction.

For the purpose of background rejection, we require that all three charged tracks should enter the ECAL/muon filter for a successful PID. Energy loss for charged particles pene-

Variable	Selection Criteria
Decay z coordinate	$25{\rm mm} < z < 140{\rm mm}$
Decay daughter energy	$> 1 \mathrm{GeV}$
Decay daughter opening angle	> 1 mrad
Charged track geometry	Hit all 3 trackers
Modules	Last 5

Table 2: Event selection criteria for our proposed search. In our numerical results, these requirements are imposed on our signal and background MC events. These criteria ensure that SM backgrounds are negligible for our signal of interest (see Supplemental Material for a discussion).

trating materials may significantly impact the PID efficiency. For example, an electron with energy 1 GeV will lose approximately 5% of its energy when passing through one single Be target, see Ref. [48, 49] for more details. For this reason, we only use the last 5 modules of the streamline as a conservative choice. Charged tracks that pass through all three tracking stations in these modules are guaranteed to be within the angular acceptance of the ECAL. An energy threshold of 1 GeV is applied to the muon and the electron-positron pair from displaced decay as a mimic of the detector response to avoid potential reconstruction errors.

We summarize the proposed search strategy in Table 2.

3.3 Signal Event Generation

To evaluate the sensitivity of MUonE to hidden vector bosons, we generate 20000 $\mu^- N \to \mu^- NV$ and $\mu^- e^- \to \mu^- e^- V$ events with a beam energy of 160 GeV using MadGraph 3.2 [50–53], with the model files constructed by FeynRules [54]. These events are weighted by the nuclear form factor, which dresses the electromagnetic vertex of the nucleus with $G(t)_2^{1/2} = \sqrt{G_2^{\rm el} + G_2^{\rm in}}$, where

$$G_2^{\text{el}}(t) = \left(\frac{a^2 t}{1 + a^2 t}\right)^2 Z^2 \left(\frac{1}{1 + t/d}\right)^2,$$
 (3.2)

$$G_2^{\text{in}}(t) = \left(\frac{a'^2 t}{1 + a'^2 t}\right)^2 Z \left(\frac{1 + t(\mu_p^2 - 1)/(4m_p^2)}{(1 + t/(0.71 \text{ GeV}^2))^4}\right)^2.$$
(3.3)

For Beryllium, $a=106Z^{-1/3}/m_e$, $d=0.164\,\mathrm{GeV}^2A^{-2/3}$ for the elastic portion and $a'=571Z^{-2/3}/m_e$ and $\mu_p=2.79$ for the inelastic portion [55, 56]. This form factor is valid in the limit $t\ll m_p^2$ [57]. The MadGraph output contains very few events that violate this condition, but nonetheless, we discard those that approach it $(t>m_p^2/2)$ by setting their weight to zero. We find that this has a negligible effect on the resulting bound.

Fig. 4 shows the production cross section for the vector gauge boson in the μe and μN channel as a function of the mass. The scaling behavior differs between the two production channels due to the inversion of the mass hierarchy between the target and beam. As shown in the plot, μe scattering dominates the cross section when the vector boson mass is

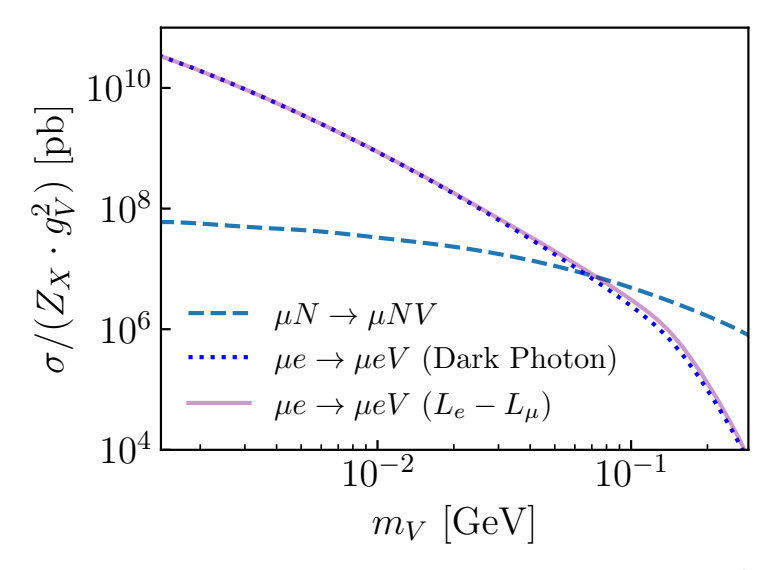


Figure 4: Production cross sections per unit charge, normalized to $g_V^2 = 1$ (Table. 1). At low masses, production from scattering off electrons is much more likely, as the electron is more likely to radiate out a gauge boson than the heavy nucleus, leading to a larger cross section. At large vector boson masses, production from nuclear scattering dominates, extending the experimental reach of MUonE to $\sim 100\text{-}150$ MeV.

below ~ 60 MeV because the target electron contributes significantly to the bremsstrahlung process, an effect which is heavily suppressed for the nuclear scattering case. On the other hand, μN scattering dominates in the large-mass regime because of the larger CoM energy for the nuclear target. With a beam energy of 160 GeV, the CoM energy in the nuclear scattering case is $\sqrt{s_{\mu N}} = 54$ GeV, compared to the electron scattering at just $\sqrt{s_{\mu e}} = 400$ MeV. The scattering off the nucleus thus enjoys a much wider available phase space, important for the production of a heavy vector boson. An important consequence of this is that adding the μN scattering significantly increases the maximum vector boson mass that MUonE is sensitive to. In addition, as noted in Section 2, the relative sign of the electron and muon couplings to the dark vector boson in the $U(1)_{L_e-L_{\mu}}$ model can change the interference between diagrams in $\mu e \to \mu eV$. Numerically, we find this effect to give an $\mathcal{O}(10)\%$ correction.

We comment on the analytical calculation of the cross section with Weizsaecker-Williams (WW) approximation [58, 59]. Using the results of Ref. [60] with the WW approximation, we find a factor of 1-2 difference in cross section with the results from MadGraph. However, we find a larger discrepancy of a factor of ~ 8 between the MadGraph result and the "Improved WW" technique used by Ref. [61] to construct analytic MUonE bounds. This discrepancy could be explained by the assumption that $m_{beam} \ll m_{A'}$ that is necessary for the derivation of the cross section in Ref. [60] (see e.g. Ref [57]), but invalid for the muon-flavored beam used by MUonE. The difference in predicted cross sections partly explains the difference in projected sensitivities in this work and in Ref. [61], with the other differences discussed in Sec. 4.

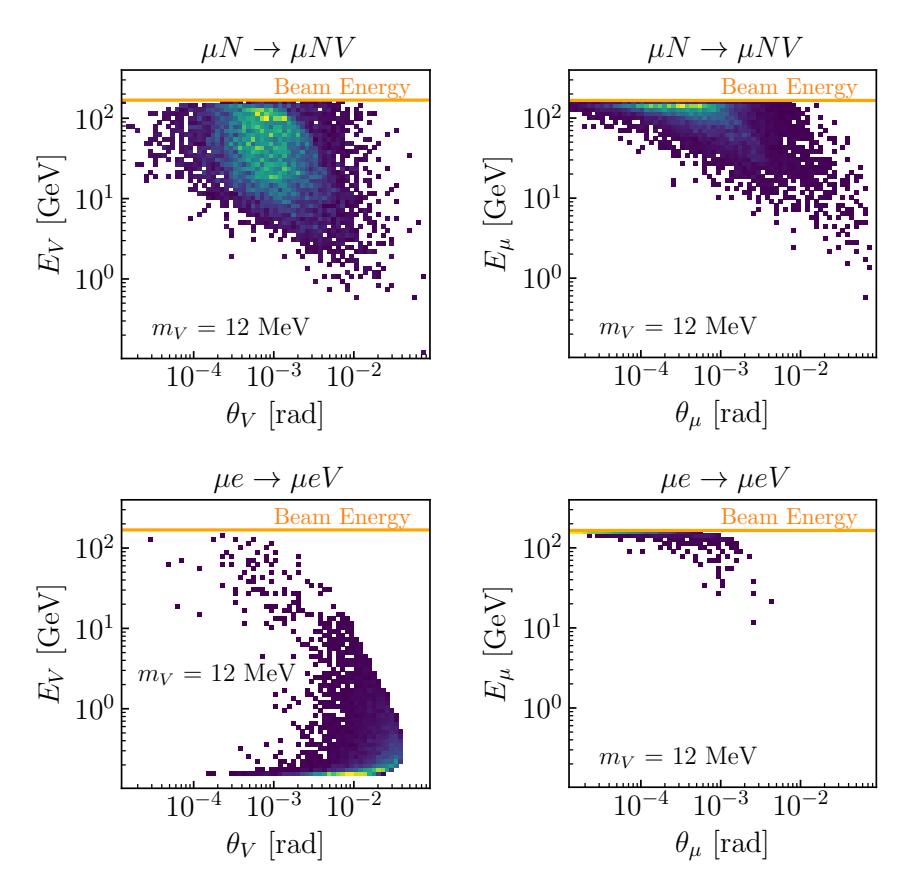


Figure 5: Energy and angle distribution for the produced vector boson and deflected muon for $m_{A'} = 12$ MeV.

Figs. 5 and 6 display the kinematic distributions of the products in $\mu e \to \mu eV$ and $\mu N \to \mu NV$ scatterings for $m_V = 12$ MeV and $m_V = 44$ MeV. As seen in the figures, scattering off electrons produces much softer vector gauge bosons than those produced from scattering off nuclei. The energy cut of $E_{\rm prod} > 1\,{\rm GeV}$ implies that vector bosons of $E_V < 2\,{\rm GeV}$ are completely invisible. Above this threshold, the probability of passing the $E_{\rm prod}$ cut for both resulting electrons increases and smoothly approaches unity at high E_V . For $m_V = 12\,{\rm MeV}$, a significant portion of the produced vector bosons lie well below $2\,{\rm GeV}$, leading to a low detection efficiency. This offsets the much greater production cross section of the electron channel, so both channels yield a similar number of signal events, as shown later in Sec. 4. For $m_V = 44\,{\rm MeV}$, the energies of the vector bosons produced in μe scattering are above $2\,{\rm GeV}$, which improves the efficiency. However, at $m_V = 44\,{\rm MeV}$, the production cross sections for both channels are comparable, again resulting in a similar contribution to signal events from the nuclear and electron scattering channels.

After production via dark bremsstrahlung, the vector boson decays, with decay length given in Eq. 2.3. The kinematics of the decay are computed manually by boosting to the rest frame of the vector boson, where the decay occurs isotropically, and then inverse boosting. In the regions of parameter space excluded by MUonE, the $m_V < 2m_\mu$, so the only available decay modes at tree-level are to electrons or neutrinos. Electrons are the

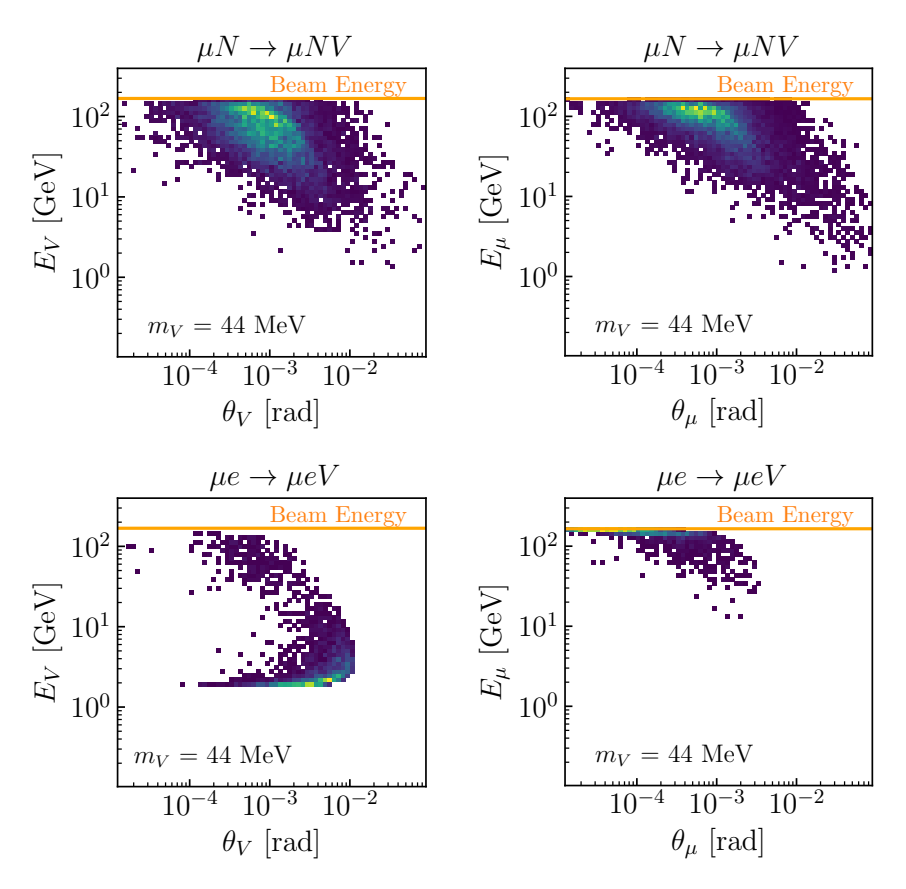


Figure 6: Energy and angle distribution for the produced vector boson and deflected muon for $m_{A'} = 44$ MeV.

only visible channel, and the visible branching ratios (for $m_A \gg 2m_e$) are 1, 2/5, 1/2 for the dark photon, $U(1)_{B-L}$, and $U(1)_{L_e-L_\mu}$ models, respectively. The lower branching ratio to visible products can slightly reduce the reach of MUonE, see Sec. 4 for a discussion. Below $m_{A'} < 2m_e$, the dark vector decays to neutrinos or is very nearly stable, and both scenarios are invisible to MUonE. After decay, the resulting visible leptons are required to pass the cuts in Table. 2, and we compile those that pass into an expected number of signal events.

3.4 Backgrounds

The background falls into two categories: (a) SM processes that happen within the target or the first tracking station and create a prompt vertex, which may be mis-reconstructed as a displaced vertex due to limited resolution. (b) SM processes that can naturally produce a displaced vertex. The first category can be safely rejected by requiring a $10\delta z$ displacement away from the target and the first tracking station, while the second category requires a simulation to examine its impact.

Ref. [33] performed a systematic, simulation-based analysis for the background process with an inclusive fourth track. It was concluded that the backgrounds can all be safely rejected. Most hadronic processes come with many extra charged particles that leave hits on the tracking stations or the ECAL, leading to rejection. The remaining small portion of events is relatively clean, and the PID system is required to reject them. The vast majority

of background events arise from $K^0 \to \pi^+\pi^-$ and $\Lambda \to p\pi^-$. The simulation finds that about 4000 such background events are expected to fake the signal topology, and can be safely rejected by ECAL as long as the per-particle-fake rate is less than 1.6%. A small number of events have $K^0 \to \pi e \nu$ or $\Lambda \to p e \nu$, where one real electron/positron is faking the displaced decay and the other is from a charged pion or proton. Simulation finds that about 8 events are expected, and can be rejected by the ECAL. Finally, about 0.5 events are expected to have two real electrons faking the displaced decay, such as $K^0 \to \pi^0\pi^0$ with one π^0 decaying into $e^+e^-\gamma$. Fortunately, all these events have at least one non-electron particle hitting the ECAL (usually a charged pion from the primary vertex, or an energetic photon), leading these events to be rejected. As a conclusion, all backgrounds can be safely rejected by our search strategy, and we assume the backgrounds are zero in our statistics.

4 Analysis and Results

Based on the discussion of Sec. 3, we perform a parameter scan over the coupling-mass plane. We generate signal event samples for 16 mass points logarithmically spaced between 2 MeV and 300 MeV. For each mass point, we apply the selection criteria on an event-by-event basis for couplings ranging from 10^{-6} –1, covering 30 logarithmically spaced points. For each parameter point, the total number of signal events is calculated by

$$N_{\text{sig}} = \epsilon_{\text{sig},N} \sigma_N \mathcal{L}_N + \epsilon_{\text{sig},e} \sigma_e \mathcal{L}_e. \tag{4.1}$$

Here $\epsilon_{\mathrm{sig},N(e)}$ is the fraction of signal events from μN (μe) scattering that pass the cuts in Table. 2, $\sigma_{N,e}$ is the production cross section calculated using MadGraph, and $\mathcal{L}_{N,e}$ is the effective luminosity. For μN scattering, $\mathcal{L}_N = 1.5 \times 10^4/8/4~\mathrm{pb}^{-1}$, while for μe scattering we have $\mathcal{L}_e = 1.5 \times 10^4/8~\mathrm{pb}^{-1}$. The factor of 8 comes from the fact that only last 5 modules can be used (Sec. 3.2), while the factor of 4 in \mathcal{L}_N comes from the Be atomic number.

Figs. 7–9 show our main results for the dark photon, $U(1)_{B-L}$ gauge boson, and $U(1)_{L_e-L_{\mu}}$ gauge boson. For each plot, we show the projected sensitivity at 95% confidence level assuming zero background from μe and μN scattering with red dotted and dashed curves, respectively. The combined result is shown with the red solid curve. In all cases, we find that the μe scattering can reach a lower coupling than the μN scattering with vector boson mass below ~ 30 MeV. This is due to the larger energy acquired by the vector boson from the Be nucleus as seen in Figs. 5 and 6, which leads to a longer decay length that should be compensated by a larger coupling. The μN scattering, on the other hand, can reach a much higher vector boson mass because of the larger CoM energy.

The existing limits are shown in the gray shaded area, while future sensitivities within the next 5 years are shown by gray dashed curves. Our recasting of these limits relies on DARKCAST [27]. We also refer the readers to Ref. [28] for a comprehensive study on U(1) vector bosons. Note that all of our searches are based on the assumption that the vector bosons only decay back to SM particles. Invisible searches, assuming decays into stable dark sector particles, do not apply.

In the following subsections, we comment on our results and emphasize the differences among these models.

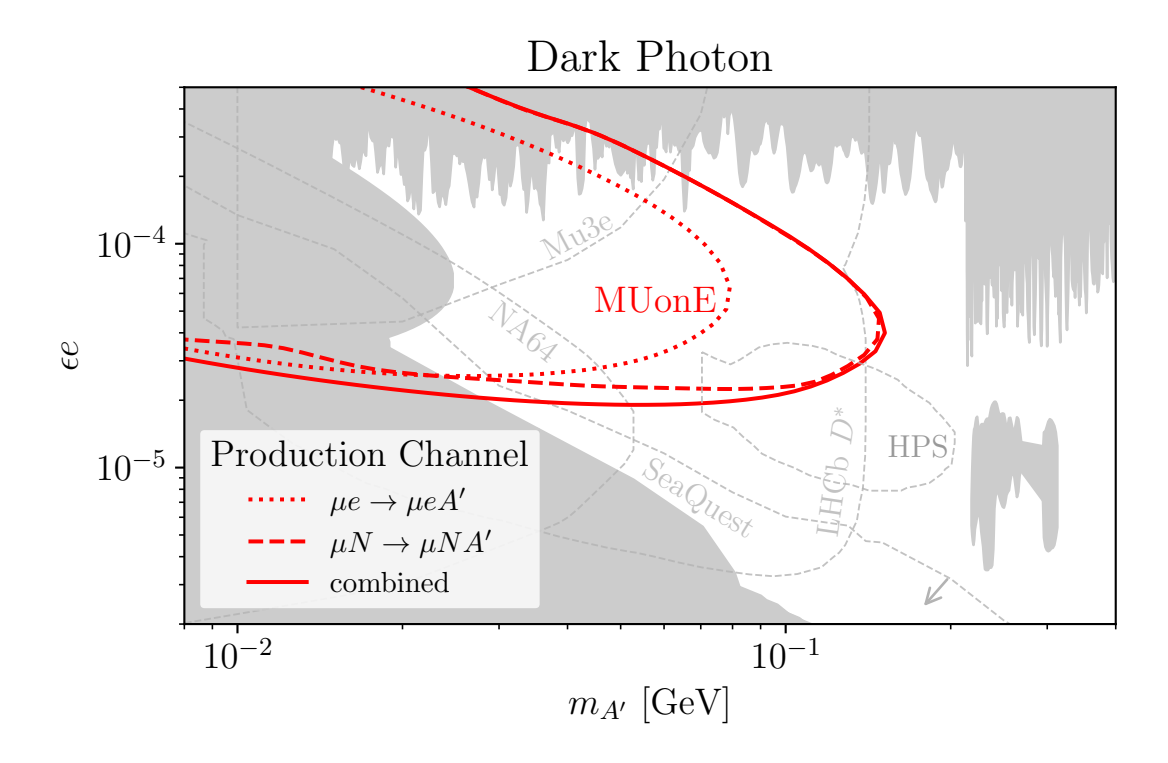


Figure 7: The result for dark photon search. MUonE sensitivity is shown with the red dotted curve (for μe scattering), the red dashed curve (for μN scattering), and the red solid curve (combined). Existing limits are shown in gray shaded regions. Selected future limits that are planned for a similar timeline as MUonE are also shown. Specifically, we add an arrow for the SeaQuest projection to indicate that it is expected to probe the parameter space below the curve.

4.1 Dark photon model

Fig. 7 shows the MUonE projection for dark photon searches. We found that the MUonE reach extends to dark photon masses as heavy as ~ 150 MeV for couplings that fall into the "gap". Note that the sensitivity is significantly smaller than that in Ref. [61]. Besides the discussion of the WW approximation in Sec. 3.3, the restriction to only the last 5 modules suppresses the luminosity. We point out that this is essential to have a reliable PID accuracy for background rejection. Existing limits are from $(g-2)_e$ [5, 62], beam dumps [57, 63–79]), electron fixed-target [80, 81], collider experiments [82–89], and rare meson decays [76, 77, 87, 88, 90–95]. Future projections shown here include HPS [96, 97], NA64e with 10^{12} electrons on target [98], D^* decay search at LHCb upgrade [99, 100], SeaQuest [101] ,and Mu3e [102].

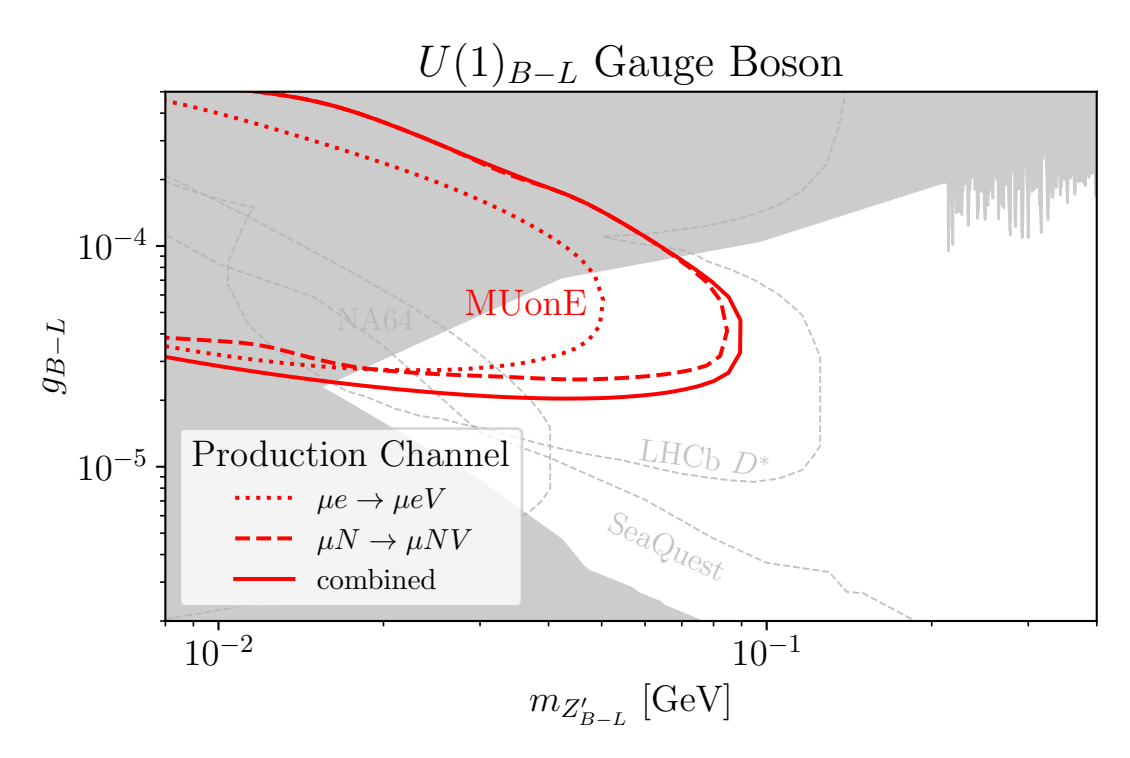


Figure 8: The result for gauged $U(1)_{B-L}$ search. MUonE sensitivity is shown with the red dotted curve (for μe scattering), the red dashed curve (for μN scattering), and the red solid curve (combined). Existing limits are shown in gray shaded regions. Selected future limits that are planned for a similar timeline as MUonE are also shown. Specifically, we add an arrow for the SeaQuest projection to indicate that it is expected to probe the parameter space below the curve.

4.2 The gauged $U(1)_{B-L}$ model

Fig. 8 shows the MUonE sensitivity to the $U(1)_{B-L}$ gauge boson. The existing dark photon limits and projections discussed in the previous subsection are re-interpreted for the $U(1)_{B-L}$ gauge boson using DARKCAST [27].

The main difference arises from the coupling to the neutrinos. This opens an additional decay channel into a neutrino pair, shortening the decay length by a factor of 2/5 compared to the dark photon model. To maintain the same decay length, the coupling must be reduced slightly, which in turn lowers the cross section. Moreover, since neutrinos are invisible, the observable signal rate is further suppressed by the branching ratio into e^+e^- , which carries the same factor of 2/5. As a result, the largest coupling that is accessible for MUonE for a given mass drops by an $\mathcal{O}(1)$ factor, and the maximum mass also reduces to about 100 MeV, slightly weaker than in the dark photon case. In addition, the $U(1)_{B-L}$ gauge theory is further constrained by neutrino experiments such as Borexino [103, 104], Texono [105], CHARM II [106], SPEAR, DORIS, and PETRA [107, 108], resulting in the extra gray-shaded region for masses around a few tens of MeV. These additional limits cover the projection of Mu3e, so it is not shown in Fig. 8. We note that the HPS projection is absent due to the lack of sufficient information to translate the result into this model.

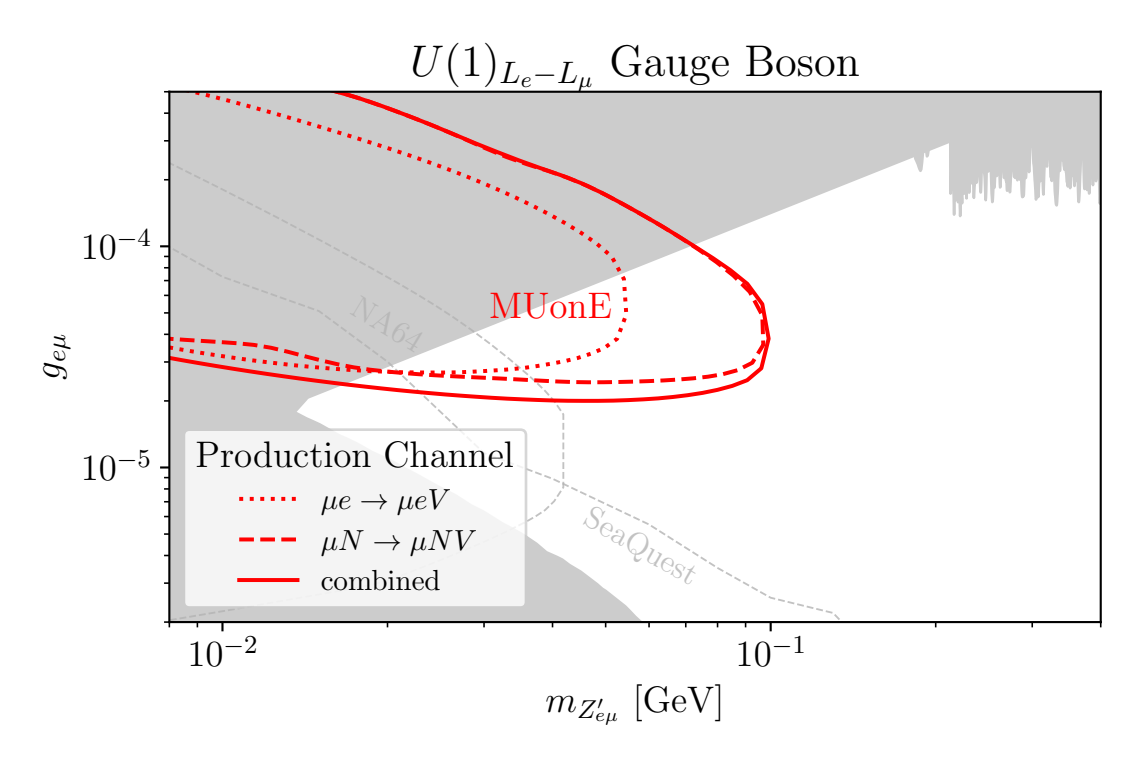


Figure 9: The result for gauged $U(1)_{L_e-L_{\mu}}$ search. MUonE sensitivity is shown with the red dotted curve (for μe scattering), the red dashed curve (for μN scattering), and the red solid curve (combined). Existing limits are shown in gray shaded regions. Selected future limits that are planned for a similar timeline as MUonE are also shown. Specifically, we add an arrow for the SeaQuest projection to indicate that it is expected to probe the parameter space below the curve.

4.3 The gauged $U(1)_{L_e-L_u}$ model

Fig. 9 shows the MUonE sensitivity for the gauged $U(1)_{L_{\mu}-L_{e}}$ model, with existing dark photon limits re-interpreted by running DARKCAST [27]. The discussion on the impact of neutrino coupling for the $U(1)_{B-L}$ model also applies here, though this gauge boson couples to one fewer neutrino flavor. This slightly enhances the sensitivity over the $U(1)_{B-L}$ case.

Unlike the previous two models, the $U(1)_{L_e-L_\mu}$ gauge boson does not couple to quarks at tree-level (although it can do so at loop-level). Consequently, the production of $U(1)_{L_\mu-L_e}$ gauge boson in hadronic experiments such as CHARM, NuCAL, and NOMAD is strongly suppressed. Nevertheless, electron beam-dump experiments have achieved similar sensitivities, so the existing bounds are not strongly affected.

The absence of a τ neutrino coupling suppresses the sensitivity of many neutrino experiments, but raises it in Super-K due to modified neutrino oscillations [109]. Among the neutrino experiments mentioned in the $U(1)_{B-L}$ case, the Texono [105] and Borexino [103, 104] remain relevant as their primary search channel is through scattering between electrons and electron neutrinos. As the $U(1)_{B-L}$ case, the Mu3e and HPS projections are absent for the reasons explained above.

5 Conclusion

In this paper, we demonstrate that the MUonE experiment provides a unique opportunity to probe hidden vector bosons through displaced decay signatures. In exploring the dark photon, $U(1)_{B-L}$, and $U(1)_{L_e-L_{\mu}}$ models as benchmark examples, we extended the prior work of Ref. [33] to include the nuclear scattering, $\mu N \to \mu NV$, in addition to the $\mu e \to \mu eV$ channel. We perform a dedicated simulation of signal events and apply the event selection criteria. Our analysis illustrates that μN scattering, owing to its higher CoM energy, substantially enhances the reach of MUonE for heavier mediators, extending the sensitivity up to $m_V \sim 150\,\mathrm{MeV}$, a factor of two improvement over the case with μe scattering alone. Together with the performance of μe scattering at low mass, the combined production channels show a promising sensitivity.

Of course, more BSM scenarios could potentially be probed at MUonE, and this work serves as a proof of concept. As MUonE approaches its data-taking phase, we hope this work provides a more solid assessment of its discovery potential, and thus motivates future explorations in the experiment.

Acknowledgement

We are grateful to Gordan Krnjaic for helpful discussions, feedback on the manuscript, and for encouraging this paper to be written. We thank Tao Han for useful comments. Fermilab is operated by Fermi Forward Discovery Group, LLC under Contract No. 89243024CSC000002 with the U.S. Department of Energy, Office of Science, Office of High Energy Physics. I.R.W. is also supported by DOE distinguished scientist fellowship grant FNAL 22-33.

References

- [1] L. B. Okun, LIMITS OF ELECTRODYNAMICS: PARAPHOTONS?, Sov. Phys. JETP 56 (1982) 502.
- [2] P. Galison and A. Manohar, TWO Z's OR NOT TWO Z's?, Phys. Lett. B 136 (1984) 279–283.
- [3] B. Holdom, Two U(1)'s and Epsilon Charge Shifts, Phys. Lett. B 166 (1986) 196-198.
- [4] C. Boehm and P. Fayet, Scalar dark matter candidates, Nucl. Phys. B 683 (2004) 219–263, [hep-ph/0305261].
- [5] M. Pospelov, Secluded U(1) below the weak scale, Phys. Rev. D 80 (2009) 095002, [0811.1030].
- [6] R. Foot, New Physics From Electric Charge Quantization?, Mod. Phys. Lett. A 6 (1991) 527–530.
- [7] X. G. He, G. C. Joshi, H. Lew, and R. R. Volkas, NEW Z-prime PHENOMENOLOGY, Phys. Rev. D 43 (1991) 22–24.
- [8] X.-G. He, G. C. Joshi, H. Lew, and R. R. Volkas, Simplest Z-prime model, Phys. Rev. D 44 (1991) 2118–2132.

- [9] R. E. Marshak and R. N. Mohapatra, Quark Lepton Symmetry and B-L as the U(1) Generator of the Electroweak Symmetry Group, Phys. Lett. B 91 (1980) 222–224.
- [10] R. N. Mohapatra and R. E. Marshak, Local B-L Symmetry of Electroweak Interactions, Majorana Neutrinos and Neutron Oscillations, Phys. Rev. Lett. 44 (1980) 1316–1319. [Erratum: Phys.Rev.Lett. 44, 1643 (1980)].
- [11] G. W. Anderson and L. J. Hall, The Electroweak phase transition and baryogenesis, Phys. Rev. D 45 (1992) 2685–2698.
- [12] M. Pietroni, The Electroweak phase transition in a nonminimal supersymmetric model, Nucl. Phys. B 402 (1993) 27–45, [hep-ph/9207227].
- [13] J. R. Espinosa and M. Quiros, *The Electroweak phase transition with a singlet, Phys. Lett.* B 305 (1993) 98–105, [hep-ph/9301285].
- [14] J. McDonald, Electroweak baryogenesis and dark matter via a gauge singlet scalar, Phys. Lett. B 323 (1994) 339–346.
- [15] J. Choi and R. R. Volkas, Real Higgs singlet and the electroweak phase transition in the Standard Model, Phys. Lett. B 317 (1993) 385–391, [hep-ph/9308234].
- [16] S. W. Ham, Y. S. Jeong, and S. K. Oh, Electroweak phase transition in an extension of the standard model with a real Higgs singlet, J. Phys. G 31 (2005), no. 8 857–871, [hep-ph/0411352].
- [17] B. Patt and F. Wilczek, Higgs-field portal into hidden sectors, hep-ph/0605188.
- [18] D. O'Connell, M. J. Ramsey-Musolf, and M. B. Wise, Minimal Extension of the Standard Model Scalar Sector, Phys. Rev. D 75 (2007) 037701, [hep-ph/0611014].
- [19] R. Essig et al., Working Group Report: New Light Weakly Coupled Particles, in Snowmass 2013: Snowmass on the Mississippi, 10, 2013. 1311.0029.
- [20] J. Alexander et al., Dark Sectors 2016 Workshop: Community Report, 8, 2016. 1608.08632.
- [21] M. Battaglieri et al., US Cosmic Visions: New Ideas in Dark Matter 2017: Community Report, in U.S. Cosmic Visions: New Ideas in Dark Matter, 7, 2017. 1707.04591.
- [22] J. Beacham et al., Physics Beyond Colliders at CERN: Beyond the Standard Model Working Group Report, J. Phys. G 47 (2020), no. 1 010501, [1901.09966].
- [23] J. Alimena et al., Searching for long-lived particles beyond the Standard Model at the Large Hadron Collider, J. Phys. G 47 (2020), no. 9 090501, [1903.04497].
- [24] D. Acosta et al., Review of opportunities for new long-lived particle triggers in Run 3 of the Large Hadron Collider, 2110.14675.
- [25] N. Bernal, M. Heikinheimo, T. Tenkanen, K. Tuominen, and V. Vaskonen, The Dawn of FIMP Dark Matter: A Review of Models and Constraints, Int. J. Mod. Phys. A 32 (2017), no. 27 1730023, [1706.07442].
- [26] D. Curtin et al., Long-Lived Particles at the Energy Frontier: The MATHUSLA Physics Case, Rept. Prog. Phys. 82 (2019), no. 11 116201, [1806.07396].
- [27] P. Ilten, Y. Soreq, M. Williams, and W. Xue, Serendipity in dark photon searches, JHEP 06 (2018) 004, [1801.04847].
- [28] M. Bauer, P. Foldenauer, and J. Jaeckel, Hunting All the Hidden Photons, JHEP 07 (2018) 094, [1803.05466].

- [29] M. Graham, C. Hearty, and M. Williams, Searches for Dark Photons at Accelerators, Ann. Rev. Nucl. Part. Sci. 71 (2021) 37–58, [2104.10280].
- [30] G. Krnjaic, Testing Thermal-Relic Dark Matter with a Dark Photon Mediator, 2505.04626.
- [31] MUonE Collaboration, G. Abbiendi et al., Measuring the leading hadronic contribution to the muon g-2 via µe scattering, Eur. Phys. J. C 77 (2017), no. 3 139, [1609.08987].
- [32] MUonE Collaboration, Letter of Intent: the MUonE project, .
- [33] I. Galon, D. Shih, and I. R. Wang, Dark photons and displaced vertices at the MUonE experiment, Phys. Rev. D 107 (2023), no. 9 095003, [2202.08843].
- [34] G. Krnjaic, D. Rocha, and I. R. Wang, Discovering Dark Matter with the MUonE Experiment, Phys. Rev. Lett. 134 (2025), no. 16 161801, [2409.00170].
- [35] U. Marconi and C. Matteuzi, "Private communication."
- [36] B. Holdom, Searching for ϵ Charges and a New U(1), Phys. Lett. B 178 (1986) 65–70.
- [37] S. R. Amendolia et al., A Measurement of the Pion Charge Radius, Phys. Lett. B 146 (1984) 116–120.
- [38] NA7 Collaboration, S. R. Amendolia et al., A Measurement of the Space Like Pion Electromagnetic Form-Factor, Nucl. Phys. B 277 (1986) 168.
- [39] S. Borsanyi et al., Leading hadronic contribution to the muon magnetic moment from lattice QCD, Nature 593 (2021), no. 7857 51–55, [2002.12347].
- [40] T. Aoyama et al., The anomalous magnetic moment of the muon in the Standard Model, Phys. Rept. 887 (2020) 1–166, [2006.04822].
- [41] A. Boccaletti et al., High precision calculation of the hadronic vacuum polarisation contribution to the muon anomaly, 2407.10913.
- [42] Muon g-2 Collaboration, G. W. Bennett *et al.*, Final Report of the Muon E821 Anomalous Magnetic Moment Measurement at BNL, Phys. Rev. D 73 (2006) 072003, [hep-ex/0602035].
- [43] Muon g-2 Collaboration, B. Abi et al., Measurement of the Positive Muon Anomalous Magnetic Moment to 0.46 ppm, Phys. Rev. Lett. 126 (2021), no. 14 141801, [2104.03281].
- [44] Muon g-2 Collaboration, D. P. Aguillard et al., Measurement of the Positive Muon Anomalous Magnetic Moment to 0.20 ppm, Phys. Rev. Lett. 131 (2023), no. 16 161802, [2308.06230].
- [45] P. Banerjee et al., Theory for muon-electron scattering @ 10 ppm: A report of the MUonE theory initiative, Eur. Phys. J. C 80 (2020), no. 6 591, [2004.13663].
- [46] CMS Collaboration, The Phase-2 Upgrade of the CMS Tracker, Tech. Rep. CERN-LHCC-2017-009, CMS-TDR-014, CERN, Geneva, 2017.
- [47] CMS Collaboration, E. Migliore, Status of the upgrade project of the CMS Tracker for HL-LHC, Tech. Rep. 10, CERN, Geneva, 2022.
- [48] R. Walters, Stopping-power & range tables for electrons, protons, and helium ions, NIST Standard Reference Database 124, NIST (2017).
- [49] Particle Data Group Collaboration, S. Navas et al., Review of particle physics, Phys. Rev. D 110 (2024), no. 3 030001.

- [50] J. Alwall, M. Herquet, F. Maltoni, O. Mattelaer, and T. Stelzer, MadGraph 5: Going Beyond, JHEP 06 (2011) 128, [1106.0522].
- [51] J. Alwall, R. Frederix, S. Frixione, V. Hirschi, F. Maltoni, O. Mattelaer, H. S. Shao, T. Stelzer, P. Torrielli, and M. Zaro, The automated computation of tree-level and next-to-leading order differential cross sections, and their matching to parton shower simulations, JHEP 07 (2014) 079, [1405.0301].
- [52] S. Frixione, O. Mattelaer, M. Zaro, and X. Zhao, Lepton collisions in MadGraph5 aMC@NLO, 2108.10261.
- [53] O. Mattelaer and K. Ostrolenk, Speeding up MadGraph5_aMC@NLO, Eur. Phys. J. C 81 (2021), no. 5 435, [2102.00773].
- [54] A. Alloul, N. D. Christensen, C. Degrande, C. Duhr, and B. Fuks, FeynRules 2.0 A complete toolbox for tree-level phenomenology, Comput. Phys. Commun. 185 (2014) 2250–2300, [1310.1921].
- [55] C.-Y. Chen, M. Pospelov, and Y.-M. Zhong, Muon Beam Experiments to Probe the Dark Sector, Phys. Rev. D 95 (2017), no. 11 115005, [1701.07437].
- [56] Y.-S. Tsai, Pair Production and Bremsstrahlung of Charged Leptons, Rev. Mod. Phys. 46 (1974) 815. [Erratum: Rev.Mod.Phys. 49, 421–423 (1977)].
- [57] J. D. Bjorken, R. Essig, P. Schuster, and N. Toro, New fixed-target experiments to search for dark gauge forces, Phys. Rev. D80 (2009) 075018, [0906.0580].
- [58] C. F. von Weizsacker, Radiation emitted in collisions of very fast electrons, Z. Phys. 88 (1934) 612–625.
- [59] E. J. Williams, Nature of the high-energy particles of penetrating radiation and status of ionization and radiation formulae, Phys. Rev. 45 (1934) 729–730.
- [60] Y.-S. Liu and G. A. Miller, Validity of the Weizsäcker-Williams approximation and the analysis of beam dump experiments: Production of an axion, a dark photon, or a new axial-vector boson, Phys. Rev. D 96 (2017), no. 1 016004, [1705.01633].
- [61] G. Grilli di Cortona and E. Nardi, Probing light mediators at the MUonE experiment, Phys. Rev. D 105 (2022), no. 11 L111701, [2204.04227].
- [62] M. Endo, K. Hamaguchi, and G. Mishima, Constraints on Hidden Photon Models from Electron g-2 and Hydrogen Spectroscopy, Phys. Rev. D86 (2012) 095029, [1209.2558].
- [63] E. M. Riordan et al., Search for short-lived axions in an electron-beam-dump experiment, Phys. Rev. Lett. **59** (1987) 755.
- [64] J. D. Bjorken, S. Ecklund, W. R. Nelson, A. Abashian, C. Church, B. Lu, L. W. Mo, T. A. Nunamaker, and P. Rassmann, Search for neutral metastable penetrating particles produced in the SLAC beam dump, Phys. Rev. D38 (1988) 3375.
- [65] A. Bross, M. Crisler, S. H. Pordes, J. Volk, S. Errede, and J. Wrbanek, A search for short-lived particles produced in an electron beam dump, Phys. Rev. Lett. 67 (1991) 2942–2945.
- [66] A. Konaka et al., Search for neutral particles in electron-beam-dump experiment, Phys. Rev. Lett. 57 (1986) 659.
- [67] M. Davier and H. Nguyen Ngoc, An unambiguous search for a light Higgs boson, Phys. Lett. B229 (1989) 150.

- [68] S. Andreas, C. Niebuhr, and A. Ringwald, New Limits on Hidden Photons from Past Electron Beam Dumps, Phys. Rev. D86 (2012) 095019, [1209.6083].
- [69] J. Blümlein et al., Limits on neutral light scalar and pseudoscalar particles in a proton beam dump experiment, Z. Phys. C51 (1991) 341–350.
- [70] J. Blümlein et al., Limits on the mass of light (pseudo)scalar particles from Bethe-Heitler e⁺e⁻ and μ⁺μ⁻ pair production in a proton-iron beam dump experiment, Int. J. Mod. Phys. A7 (1992) 3835–3850.
- [71] J. Blümlein and J. Brunner, New exclusion limits for dark gauge forces from beam-dump data, Phys. Lett. B701 (2011) 155–159, [1104.2747].
- [72] J. Blümlein and J. Brunner, New exclusion limits on dark gauge forces from proton bremsstrahlung in beam-dump data, Phys. Lett. B731 (2014) 320–326, [1311.3870].
- [73] CHARM Collaboration, F. Bergsma et al., Search for Axion Like Particle Production in 400-GeV Proton Copper Interactions, Phys. Lett. 157B (1985) 458-462.
- [74] S. Gninenko, Constraints on sub-GeV hidden sector gauge bosons from a search for heavy neutrino decays, Phys. Lett. B713 (2012) 244–248, [1204.3583].
- [75] NOMAD Collaboration, P. Astier et al., Search for heavy neutrinos mixing with tau neutrinos, Phys. Lett. B506 (2001) 27–38, [hep-ex/0101041].
- [76] G. Bernardi et al., Search for neutrino decay, Phys. Lett. B166 (1986) 479.
- [77] S. Gninenko, Stringent limits on the $\pi^0 \to \gamma X, X \to e^+e^-$ decay from neutrino experiments and constraints on new light gauge bosons, Phys. Rev. **D85** (2012) 055027, [1112.5438].
- [78] NA64 Collaboration, D. Banerjee et al., Search for a Hypothetical 16.7 MeV Gauge Boson and Dark Photons in the NA64 Experiment at CERN, Phys. Rev. Lett. 120 (2018), no. 23 231802, [1803.07748].
- [79] **NA64 Collaboration**, D. Banerjee *et al.*, *Improved limits on a hypothetical X(16.7) boson* and a dark photon decaying into e^+e^- pairs, Phys. Rev. D **101** (2020), no. 7 071101, [1912.11389].
- [80] A1 Collaboration, H. Merkel et al., Search at the Mainz Microtron for light massive gauge bosons relevant for the muon g-2 anomaly, Phys. Rev. Lett. 112 (2014) 221802, [1404.5502].
- [81] APEX Collaboration, S. Abrahamyan et al., Search for a new gauge boson in electron-nucleus fixed-target scattering by the APEX experiment, Phys. Rev. Lett. 107 (2011) 191804, [1108.2750].
- [82] **BaBar Collaboration**, B. Aubert et al., Search for dimuon decays of a light scalar boson in radiative transitions $\Upsilon \to \gamma A^0$, Phys. Rev. Lett. **103** (2009) 081803, [0905.4539].
- [83] D. Curtin et al., Exotic decays of the 125 GeV Higgs boson, Phys. Rev. D90 (2014) 075004, [1312.4992].
- [84] **BaBar Collaboration**, J. P. Lees et al., Search for a dark photon in e^+e^- collisions at BaBar, Phys. Rev. Lett. **113** (2014) 201801, [1406.2980].
- [85] **BESIII Collaboration**, M. Ablikim et al., Dark photon search in the mass range between 1.5 and 3.4 GeV/c^2 , 1705.04265.
- [86] LHCb Collaboration, R. Aaij et al., Search for dark photons produced in 13 TeV pp collisions, 1710.02867.

- [87] KLOE-2 Collaboration, F. Archilli et al., Search for a vector gauge boson in φ meson decays with the KLOE detector, Phys. Lett. B706 (2012) 251–255, [1110.0411].
- [88] **KLOE-2 Collaboration**, A. Anastasi et al., Limit on the production of a new vector boson in $e^+e^- \to U\gamma$, $U \to \pi^+\pi^-$ with the KLOE experiment, Phys. Lett. **B757** (2016) 356–361, [1603.06086].
- [89] FASER Collaboration, H. Abreu et al., Search for dark photons with the FASER detector at the LHC, Phys. Lett. B 848 (2024) 138378, [2308.05587].
- [90] SINDRUM I Collaboration, R. Meijer Drees et al., Search for weakly interacting neutral bosons produced in π⁻p interactions at rest and decaying into e⁺e⁻ pairs, Phys. Rev. Lett.
 68 (1992) 3845–3848.
- [91] KLOE-2 Collaboration, D. Babusci et al., Limit on the production of a light vector gauge boson in φ meson decays with the KLOE detector, Phys. Lett. B720 (2013) 111–115, [1210.3927].
- [92] WASA-at-COSY Collaboration, P. Adlarson et al., Search for a dark photon in the $\pi^0 \rightarrow e^+e^-\gamma$ decay, Phys. Lett. B726 (2013) 187–193, [1304.0671].
- [93] **HADES Collaboration**, G. Agakishiev et al., Searching for a dark photon with HADES, Phys. Lett. **B731** (2014) 265–271, [1311.0216].
- [94] PHENIX Collaboration, A. Adare et al., Search for dark photons from neutral meson decays in pp and dAu collisions at $\sqrt{s_{NN}} = 200$ GeV, Phys. Rev. C91 (2015) 031901, [1409.0851].
- [95] **NA48/2 Collaboration**, J. R. Batley *et al.*, Search for the dark photon in π^0 decays, *Phys. Lett.* **B746** (2015) 178–185, [1504.00607].
- [96] **HPS Collaboration**, P. H. Adrian *et al.*, Search for a dark photon in electroproduced e^+e^- pairs with the Heavy Photon Search experiment at JLab, Phys. Rev. D **98** (2018), no. 9 091101, [1807.11530].
- [97] N. Baltzell et al., The Heavy Photon Search Experiment, 2203.08324.
- [98] S. Gninenko, Addendum to the NA64 Proposal: Search for the $A' \to invisible$ and $X \to e^+e^-$ decays in 2021, tech. rep., CERN, Geneva, 2018.
- [99] P. Ilten, J. Thaler, M. Williams, and W. Xue, Dark photons from charm mesons at LHCb, Phys. Rev. D92 (2015) 115017, [1509.06765].
- [100] P. Ilten, Y. Soreq, J. Thaler, M. Williams, and W. Xue, Proposed inclusive dark photon search at LHCb, Phys. Rev. Lett. 116 (2016) 251803, [1603.08926].
- [101] S. Gardner, R. J. Holt, and A. S. Tadepalli, New prospects in fixed target searches for dark forces with the SeaQuest experiment at Fermilab, Phys. Rev. D93 (2016) 115015, [1509.00050].
- [102] B. Echenard, R. Essig, and Y.-M. Zhong, Projections for dark photon searches at Mu3e, JHEP 01 (2015) 113, [1411.1770].
- [103] G. Bellini et al., Precision measurement of the 7Be solar neutrino interaction rate in Borexino, Phys. Rev. Lett. 107 (2011) 141302, [1104.1816].
- [104] R. Harnik, J. Kopp, and P. A. N. Machado, Exploring ν Signals in Dark Matter Detectors, JCAP 1207 (2012) 026, [1202.6073].

- [105] S. Bilmis, I. Turan, T. M. Aliev, M. Deniz, L. Singh, and H. T. Wong, Constraints on Dark Photon from Neutrino-Electron Scattering Experiments, Phys. Rev. D 92 (2015), no. 3 033009, [1502.07763].
- [106] CHARM-II Collaboration, P. Vilain et al., Measurement of differential cross-sections for muon-neutrino electron scattering, Phys. Lett. B 302 (1993) 351–355.
- [107] E. D. Carlson, Limits on a new U(1) coupling, Nucl. Phys. **B286** (1987) 378–398.
- [108] C. Frugiuele, E. Fuchs, G. Perez, and M. Schlaffer, Constraining New Physics Models with Isotope Shift Spectroscopy, Phys. Rev. **D96** (2017), no. 1 015011, [1602.04822].
- [109] M. B. Wise and Y. Zhang, Lepton Flavorful Fifth Force and Depth-dependent Neutrino Matter Interactions, JHEP 06 (2018) 053, [1803.00591].